Supporting Information

Organic-Inorganic Hybrid Hydrogel Electrolyte for High-Performance Quasi-Solid-State Zinc-Air Batteries

Mingzhu Wu,[a] Niu Huang,*[a][b] Minghui Lv,[a] Fengyi Wang,[a] Fang Ma,[a] Yihan Deng,[a] Panpan Sun,[a] Yong Zheng,[a] Wei Liu,[a] Liqun Ye*[a][c]

[a] College of Materials and Chemical Engineering, Key Laboratory of Inorganic Nonmetallic Crystalline and Energy Conversion Materials, China Three Gorges University, Yichang 443002, China

[b] Hubei Three Gorges Laboratory, Yichang 443007, China

[c] Engineering Research Center of Eco-environment in Three Gorges Reservoir Region, Ministry of Education, China Three Gorges University, Yichang 443002, China

*E-mail: huangliu.ysxf@163.com; lqye@ctgu.edu

Synthesis of TiO_2 nanoparticles

TiO_2 nanoparticles were prepared according to a previous method.[1] 2 mL of tetrabutyl titanate (TBT) was added dropwise to 60 mL of glacial acetic acid and dispersed ultrasonically for 15 min in a 100 mL Teflon-lined stainless-steel autoclave. And then, the autoclave was sealed and kept at 160 °C for 5 hours. After cooling to room temperature, the prepared samples were washed several times with ethanol and kept dry at 70 °C.

Synthesis of PANa GPE

Initially, 7.2 ml of acrylic acid was neutralized with sodium hydroxide (4 g NaOH dissolved in 13 ml of DIW) to create acrylate sodium (ANa) solution, which was stirred for 30 min. Subsequently, 6 mg of the initiator (ammonium persulfate (APS)) and 3 mg of cross-linking agent (N, N'-Methylenebisacrylamide (MBA)) were introduced to initiate the polymerization of ANa, forming PANa. The mixture was stirred at room temperature for an additional 30 min. Then, the dispersion was maintained at 70 °C for 2 hours in a sealed container, gradually transforming into hydrogel. Finally, the hydrogel was dried at 80 °C for 2 hours (container open) and soaked in an aqueous liquid electrolyte of 6 M KOH + 0.2 M $Zn(OAc)_2$ at room temperature for 12 hours to produce the PANa GPE.

Synthesis of PVA GPE

PVA GPE was prepared by dissolving 3 g of polyvinyl alcohol (PVA, Meryer) in 25 mL of DIW and stirring for 90 min at 90 °C. Then 3 g of KOH was dissolved in 5 mL of DIW, and the KOH solution was added dropwise and stirred for another 20 min. The solution was frozen (-20 °C) for 10 hours, followed by thawing at room temperature for 2 hours, and the operation was repeated 2 times to obtain PVA GPE.

Preparation of air cathodes

The Fe-NCNT@NiFe-LDH catalyst was prepared using established methods.[2]

Material characterization

The x-ray diffraction (XRD) of the $TiO_2(NH_2)$, PANa-PVP-$TiO_2(NH_2)$, PVP, and Zinc plate were analyzed using a Smartlab-9 x-ray diffractometer. The high-resolution transmission electron microscopy (HRTEM) images and energy dispersive

spectroscopy (EDS) mapping of the $TiO_2(NH_2)$ were obtained from a JEOLJEM-2100F (UHR) Field Emission Transmission Electron Microscope. The Fourier transform infrared (FTIR) spectra of PANa-PVP-$TiO_2(NH_2)$, PANa, and PVP are collected in the wavelength range of 4000-400 cm^{-1} using a Frontier NIR instrument. The scanning electron microscope (SEM) images of PANa and PANa-PVP-$TiO_2(NH_2)$ were obtained from a JEOLJSM-7500F Scanning Electron Microscope.

Performance Measurement

The uptake and retention capacity of GPEs for liquid KOH electrolytes in exposed air at 25 °C was investigated. The synthesized electrolyte membrane (mass W_0) was immersed in a liquid electrolyte solution for 24 hours (saturated). The surface liquid was then wiped off with filter paper and weighed again (mass W_1). To evaluate the electrolyte retention capacity of GPEs, which absorbed the electrolyte solution (mass of W_2) were exposed to ambient conditions to accelerate water evaporation. The weights of the samples were varied with time (W_3). The electrolyte uptake (W_u) and retention (W_r) values of GPEs were calculated by the following equation: [3]

$$W_u = W_1/W_0$$

$$W_r = W_3 / W_2 * 100\%$$

The AC impedance spectra (EIS) of GPEs were measured using the CHI 760E electrochemical workstation. GPEs were cut into panes with a width of 1.0 cm (W) and a length of 1.0 cm (L), and the top and bottom plane surfaces were completely contacted with copper foils, which were fixing by insulating tape. The stainless-steel electrode clip was clamped on the excess copper foil and tested in the frequency range of 0.01 H_Z to 10^6 H_Z. The ionic conductivity (σ) is obtained from the following equation: [4]

$$\sigma = T / A * R$$

Here, T denotes the thickness of the gels, A is the cross-sectional area of the gels ($A = L * W$, the cross-sectional area is the product of the length and width of the gel), and R is the resistance of the GPE.

A micro-computerized tensile testing machine (Dongguan Jingwei Environmental Testing Equipment Co., Ltd.) was used to test the mechanical properties of GPE in ambient air (25 °C). The lengths of the GPEs used in the test were 4.0 cm, the widths

were 2.0 cm, and the thicknesses was 0.30 cm as well.

Preparation and performance evaluation of quasi-solid-state flexible zinc-air batteries (QSS-FZABs)

FZABs are manufactured using a layer-by-layer process. Typically, a zinc plate and an air cathode with the Fe-NCNT@NiFe-LDH catalyst in-situ grown on a carbon cloth, are face-to-face assembled with a piece of GPE to form a sandwich-type structure, and a piece of nickel foam placed on the outside of the catalyst, serving as a current collector. A breathable bandage was then used to reinforce the structural integrity of the laminate. The batteries were tested discharge polarization, discharge curve at 1 mA cm^{-2} current density, and rate performances at 2, 5, 10, and 15 mA cm^{-2} current densities on the electrochemical workstation (CHI 760E). Constant-current charge/discharge tests were performed at a current density of 2 mA cm^{-2} using a multichannel battery test system (RAND CT2001A, Wuhan RAND Electronics Co., Ltd., China).

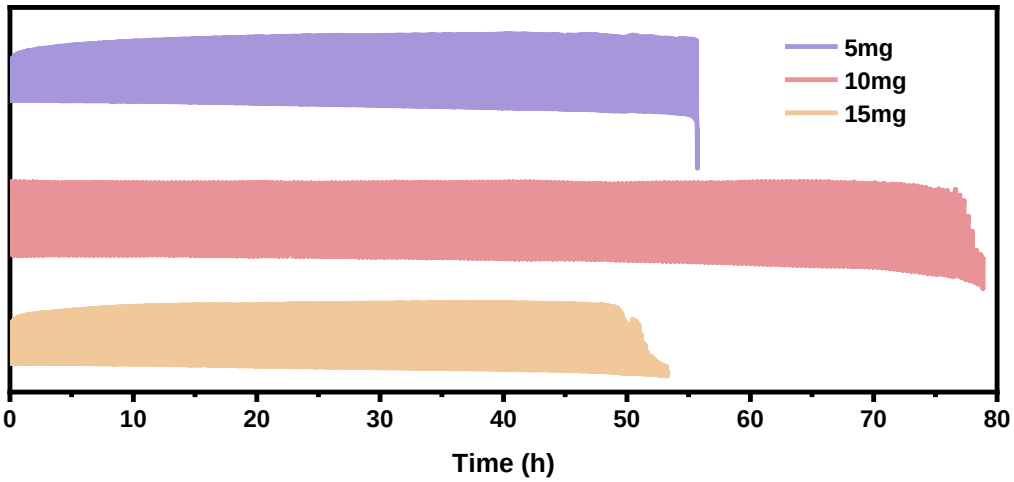

Fig. S1. Cycling curves of constant-current charge/discharge of PANa-PVP-$TiO_2(NH_2)$ GPE with different titanium dioxide contents at 2 mA cm^{-2}

Fig. S2. The optical photograph of $TiO_2(NH_2)$ nanoparticles.

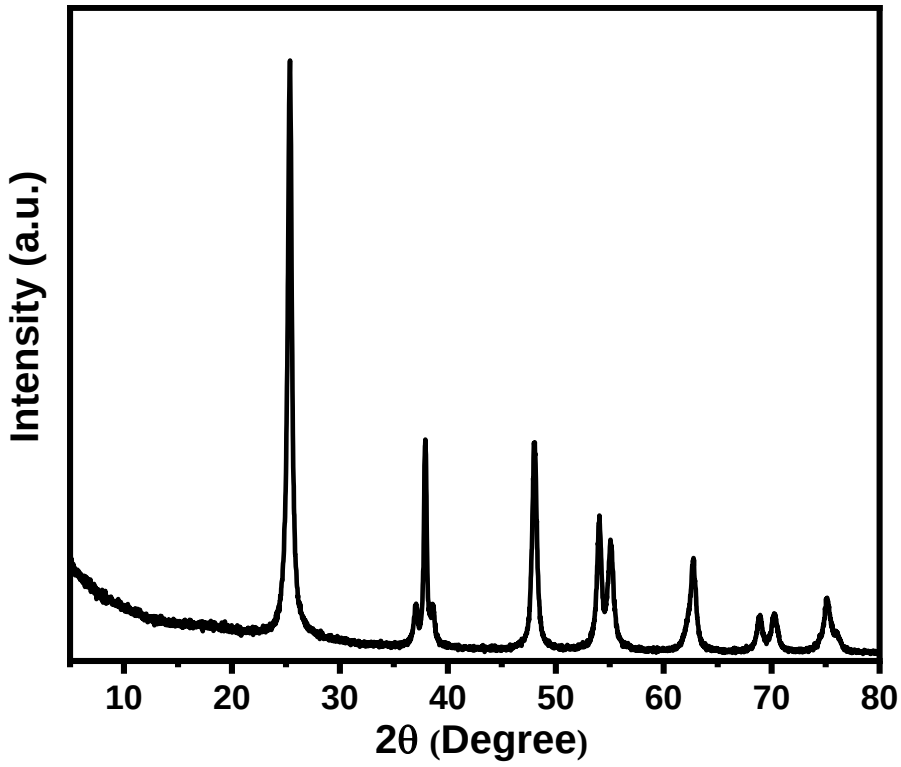

Fig. S3. XRD pattern of $TiO_2(NH_2)$ nanoparticles.

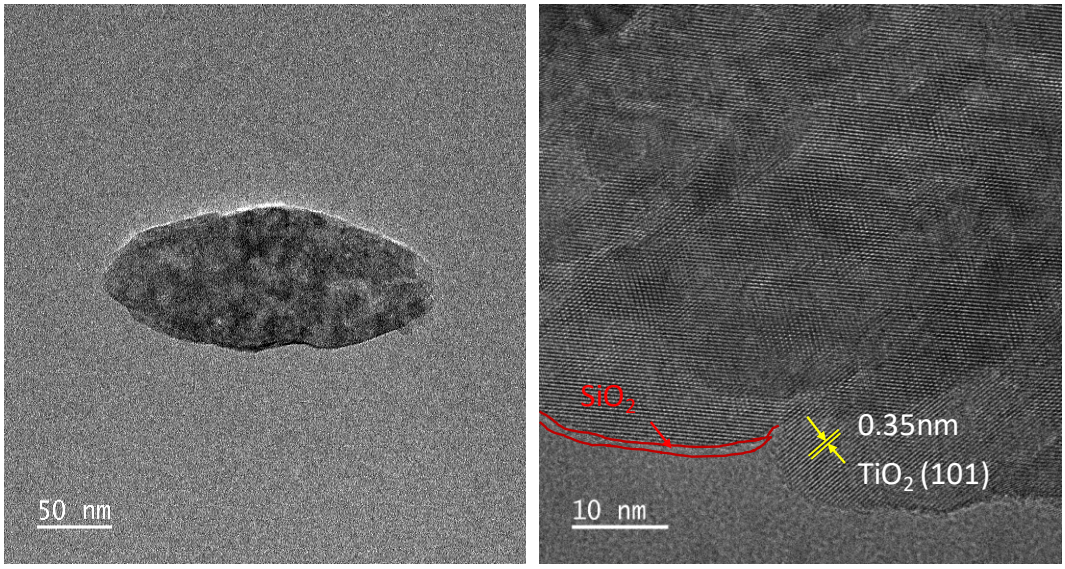

Fig. S4. High-resolution TEM images of $TiO_2(NH_2)$ nanoparticles.

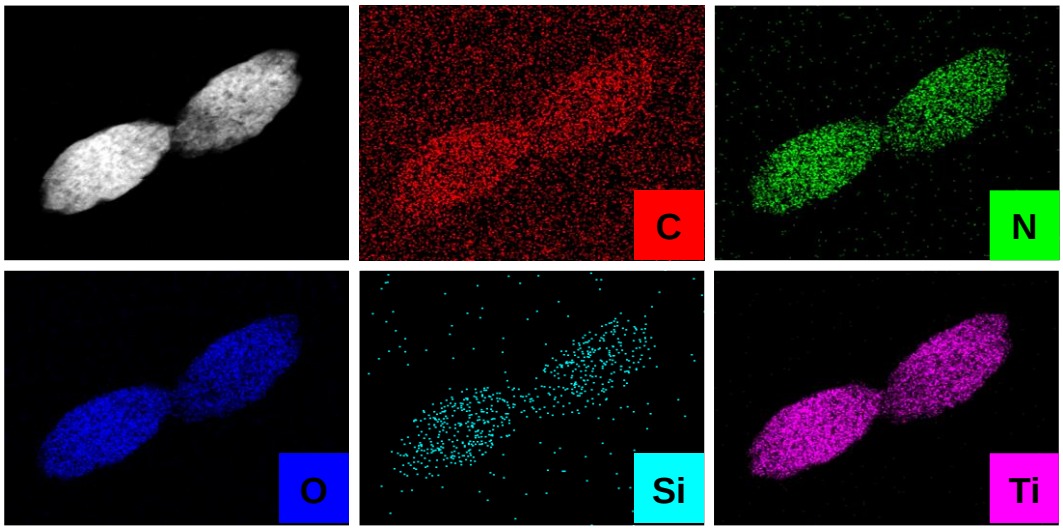

Fig. S5. EDS mapping results of $TiO_2(NH_2)$ nanoparticles.

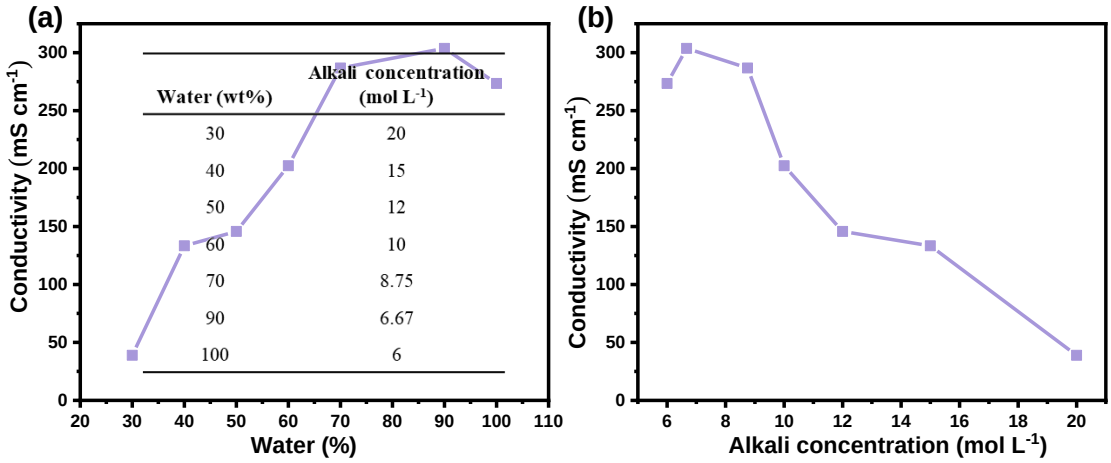

Fig. S6. (a-b) The ionic conductivity of PANa-PVP-$TiO_2(NH_2)$ GPE varied with water concentration or KOH concentration.

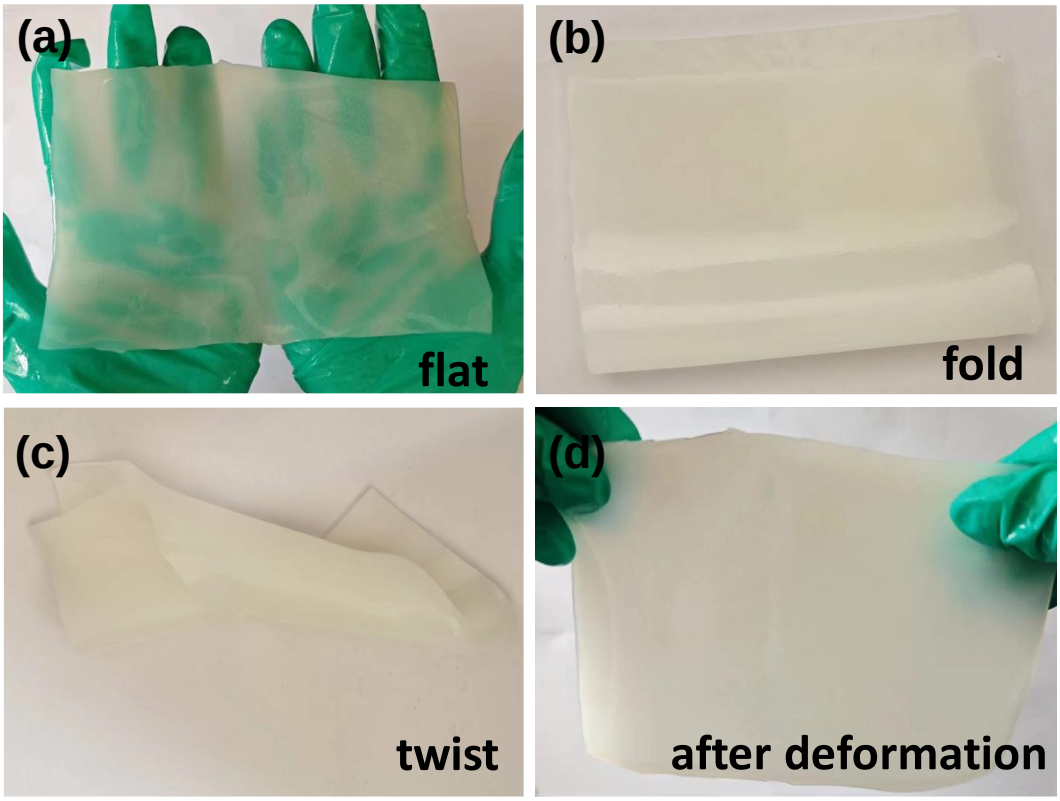

Fig. S7. Optical photographs of PANa-PVP-$TiO_2(NH_2)$ GPE in (a) flat, (b)fold, (c) twist and (d) after deformation.

Fig. S8. Optical photograph of the stretched PANa-PVP-$TiO_2(NH_2)$ GPE.

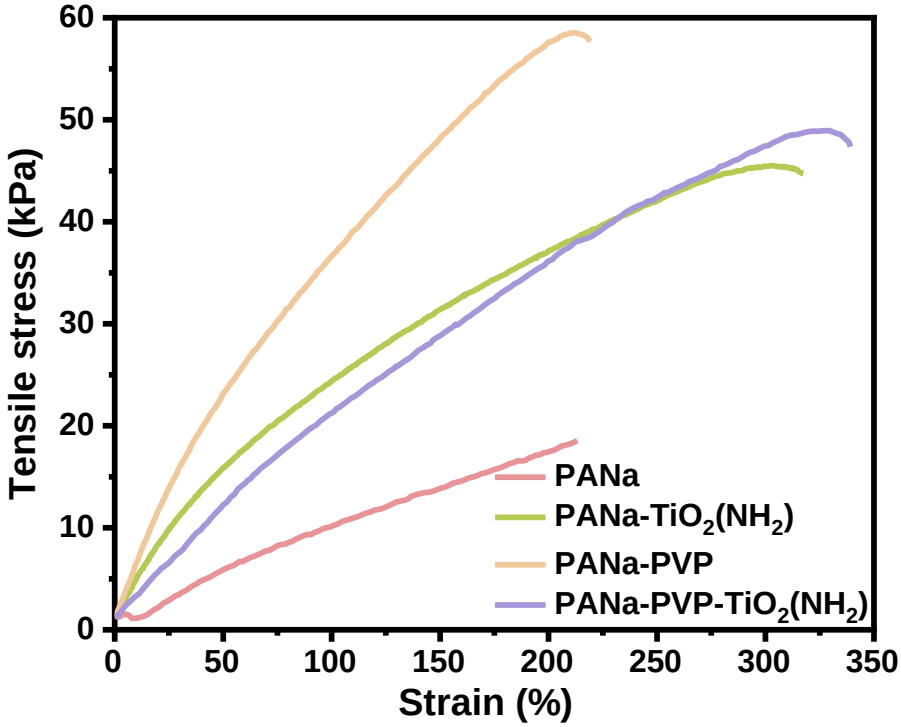

Fig. S9. Tensile properties of PANa, PANa-$TiO_2(NH_2)$, PANa-PVP, and PANa-PVP-$TiO_2(NH_2)$ GPEs.

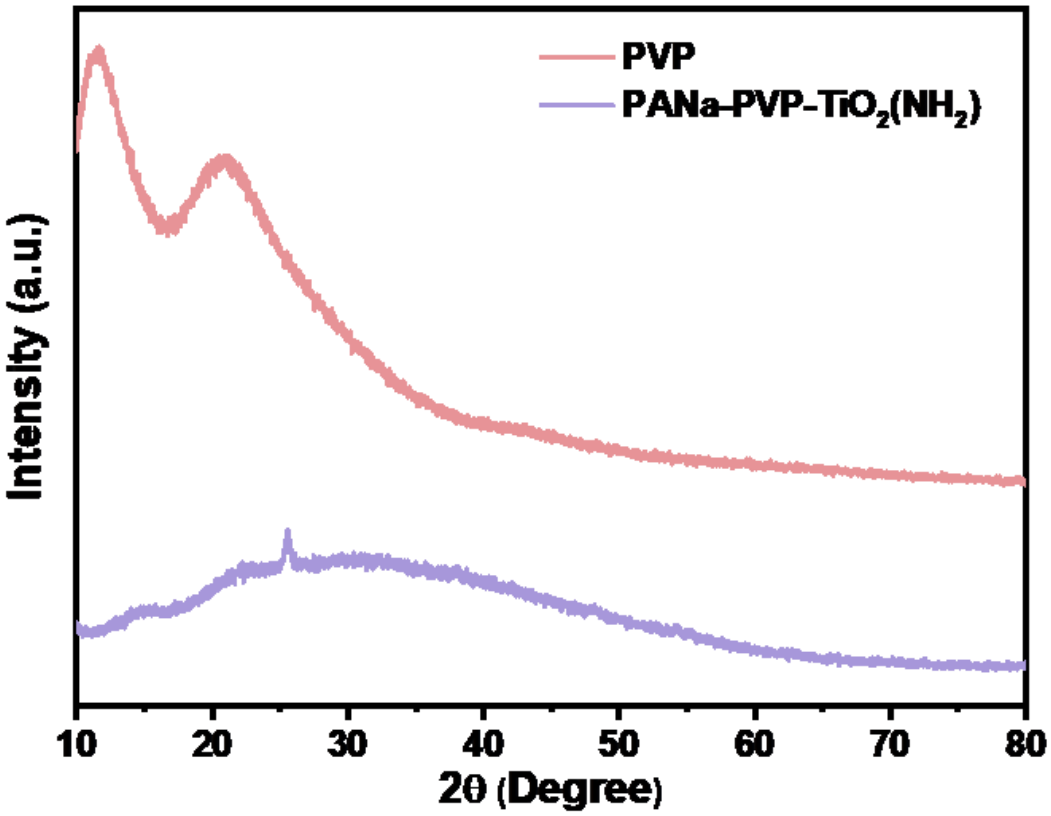

Fig. S10. XRD patterns of PVP and PANa-PVP-$TiO_2(NH_2)$.

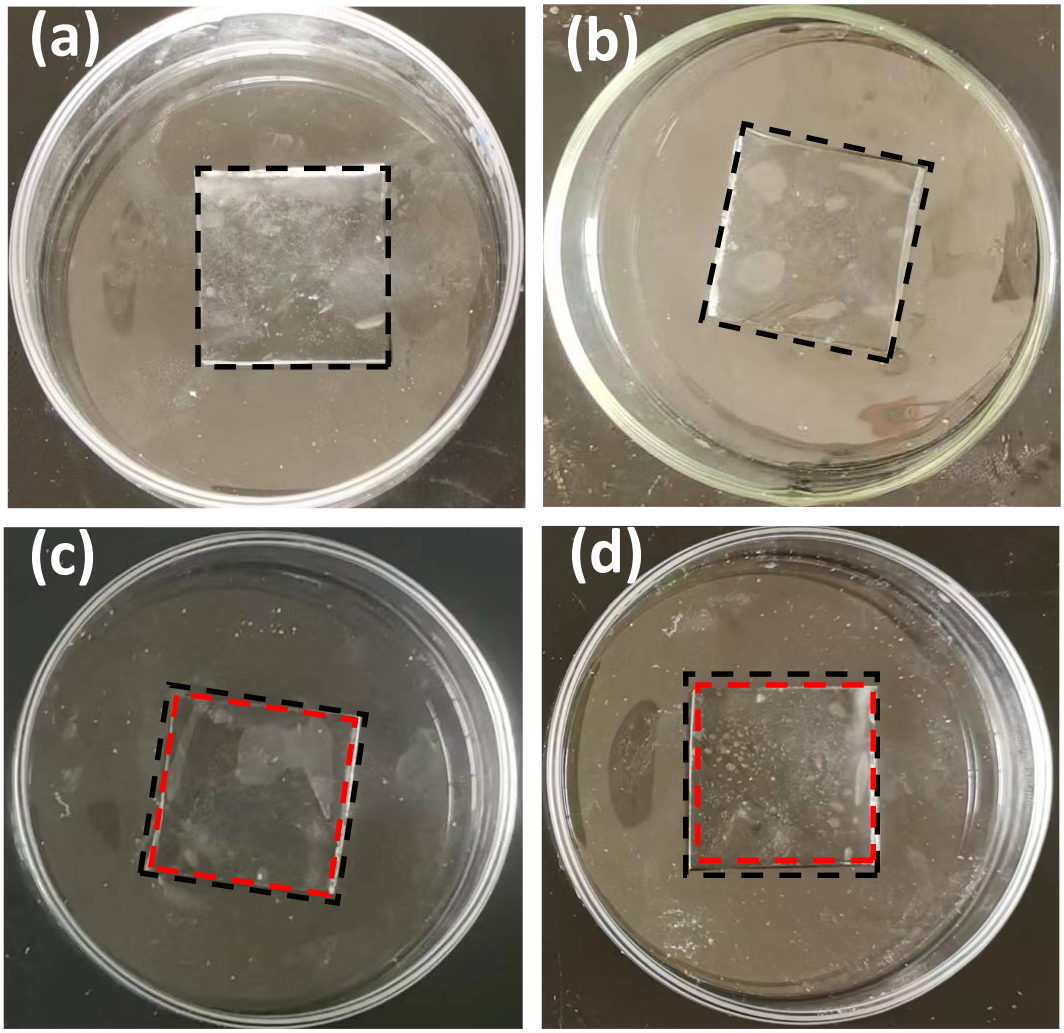

Fig. S11. Optical photos of (a) Initial PANa electrolyte and the PANa electrolyte exposed at air for (b) 24 hours, (c) 72 hours, and (d) 120 hours.

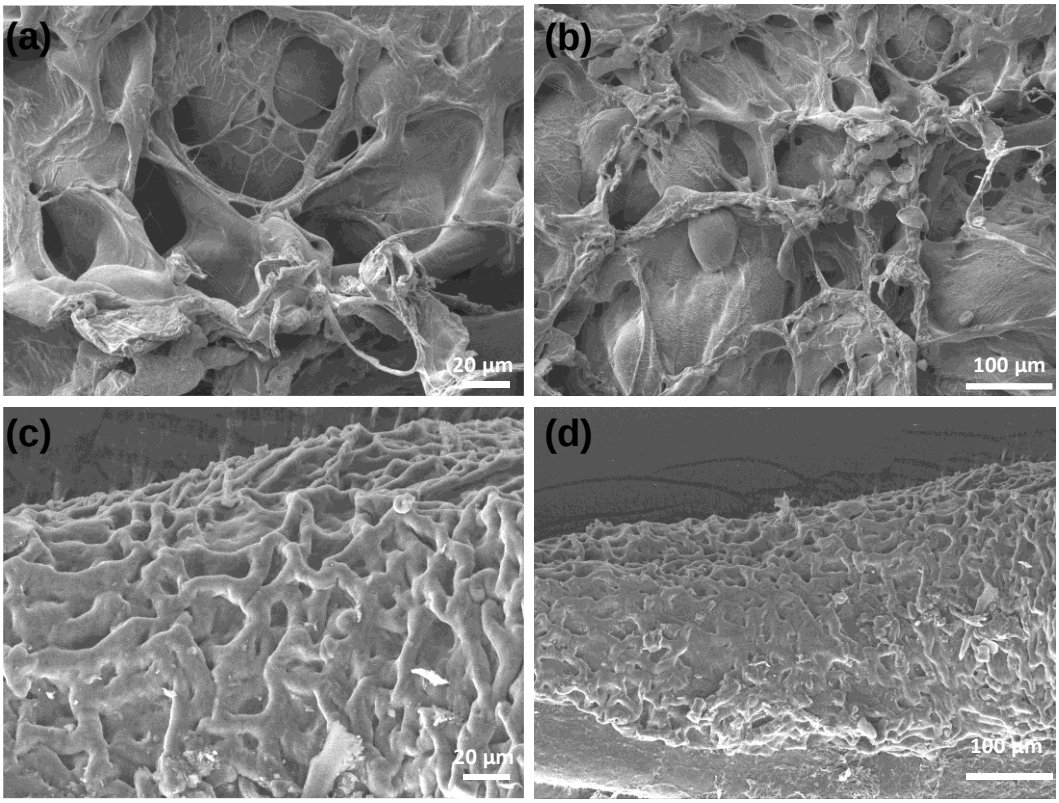

Fig. S12. SEM images of (a-b) PANa and (c-d) PANa-PVP-$TiO_2(NH_2)$ GPEs after freeze drying.

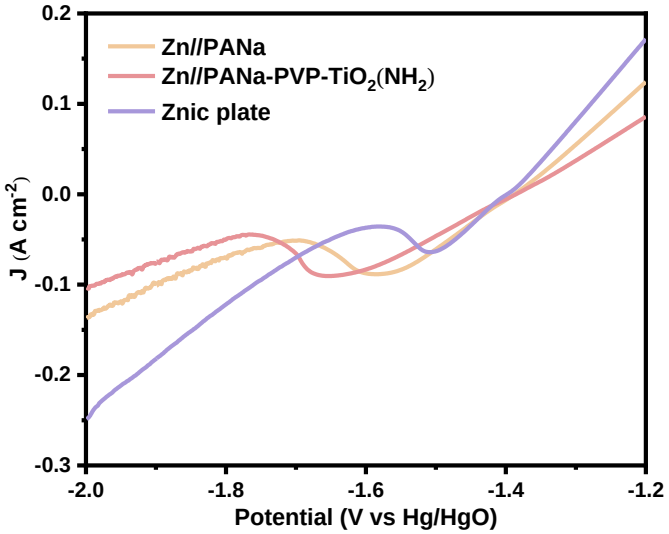

Fig. S13. Linear sweep voltammograms (LSVs) of the pure Zn plate and Zn plates coated by PANa-PVP-$TiO_2(NH_2)$ hydrogel and PANa hydrogel with 5 mV/s scanning rate, respectively.

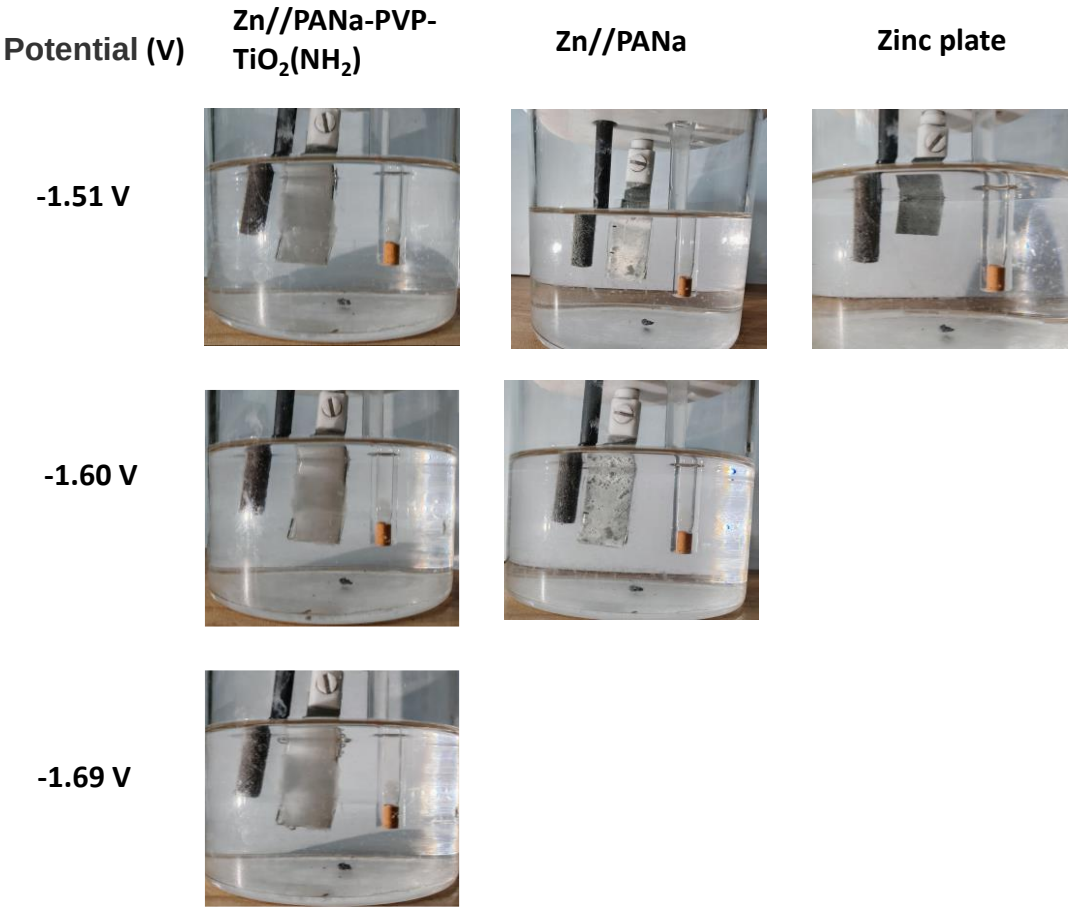

Fig. S14. Pictures of the test systems at varied working potential.

Test system: the working electrode, the Hg/HgO reference electrode, and a carbon rod as the counter electrode, with aqueous 6.0 M KOH + 0.2 M $Zn(OAc)_2$ solution as electrolyte.

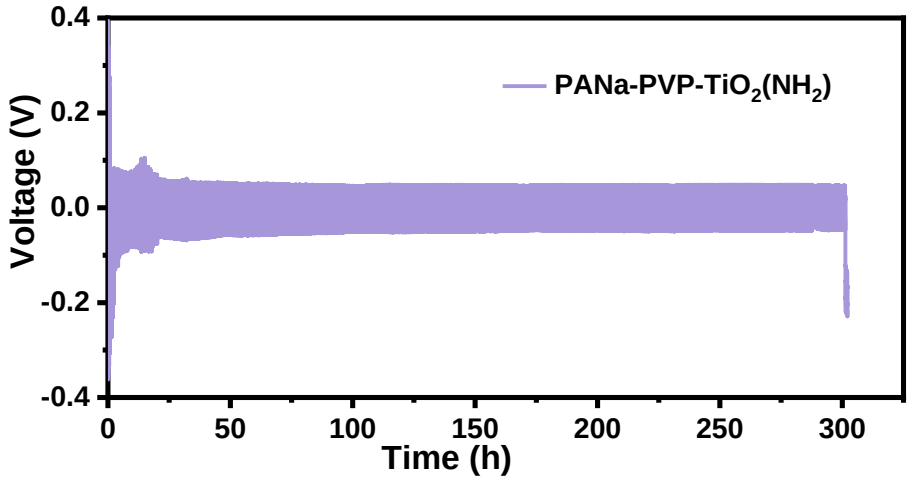

Fig. S15. Dissolution/deposition cycling of zinc in the symmetric cell assembled by using PANa-PVP-$TiO_2(NH_2)$ GPE at 5 mA cm^{-2}.

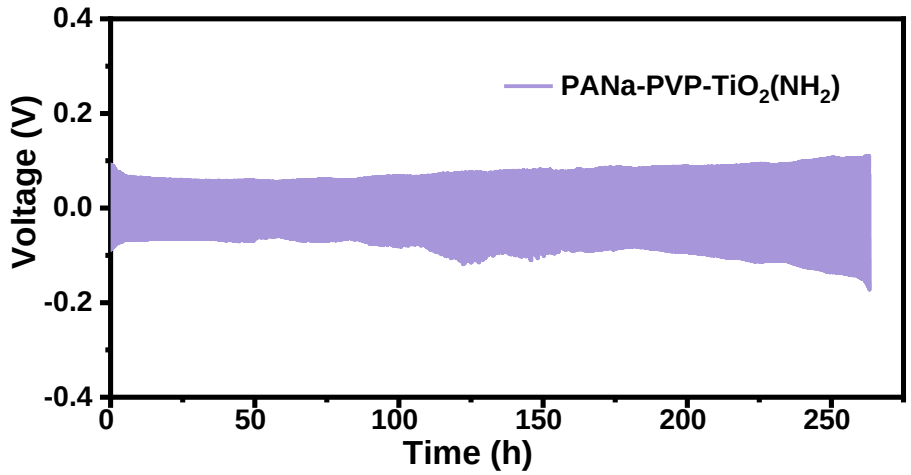

Fig. S16. Dissolution/deposition cycling of zinc in the symmetric cell assembled by using PANa-PVP-$TiO_2(NH_2)$ GPE at 10 mA cm^{-2}.

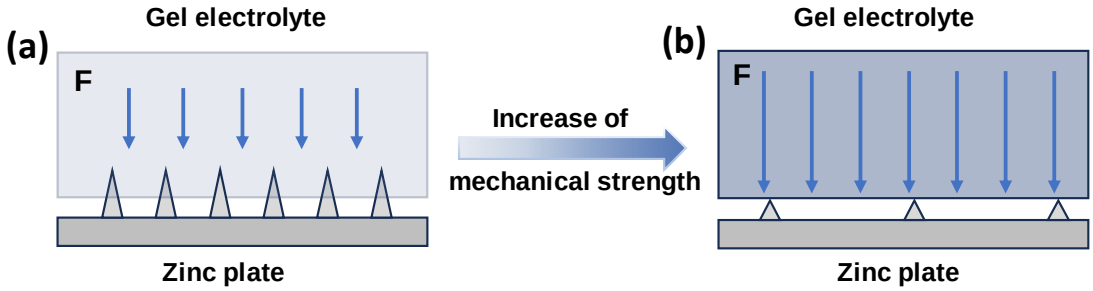

Fig. S17. Schematic representation of the inhibition effects of (a) PANa and (b) PANa-PVP-$TiO_2(NH_2)$ GPEs on zinc dendrite growth.

Figure S17 schematically shows the inhibition effects of GPEs on zinc dendrite growth. PANa GPE has poor mechanical strength, thus exerting small compressive stress on the generated dendrites (Figure S17a). In strongly contrast, PANa-PVP-$TiO_2(NH_2)$ GPE with reinforced mechanical strength exerts large compressive stress on the dendrites, thus suppressing the growth of by-products and dendrites (Figure S17b).

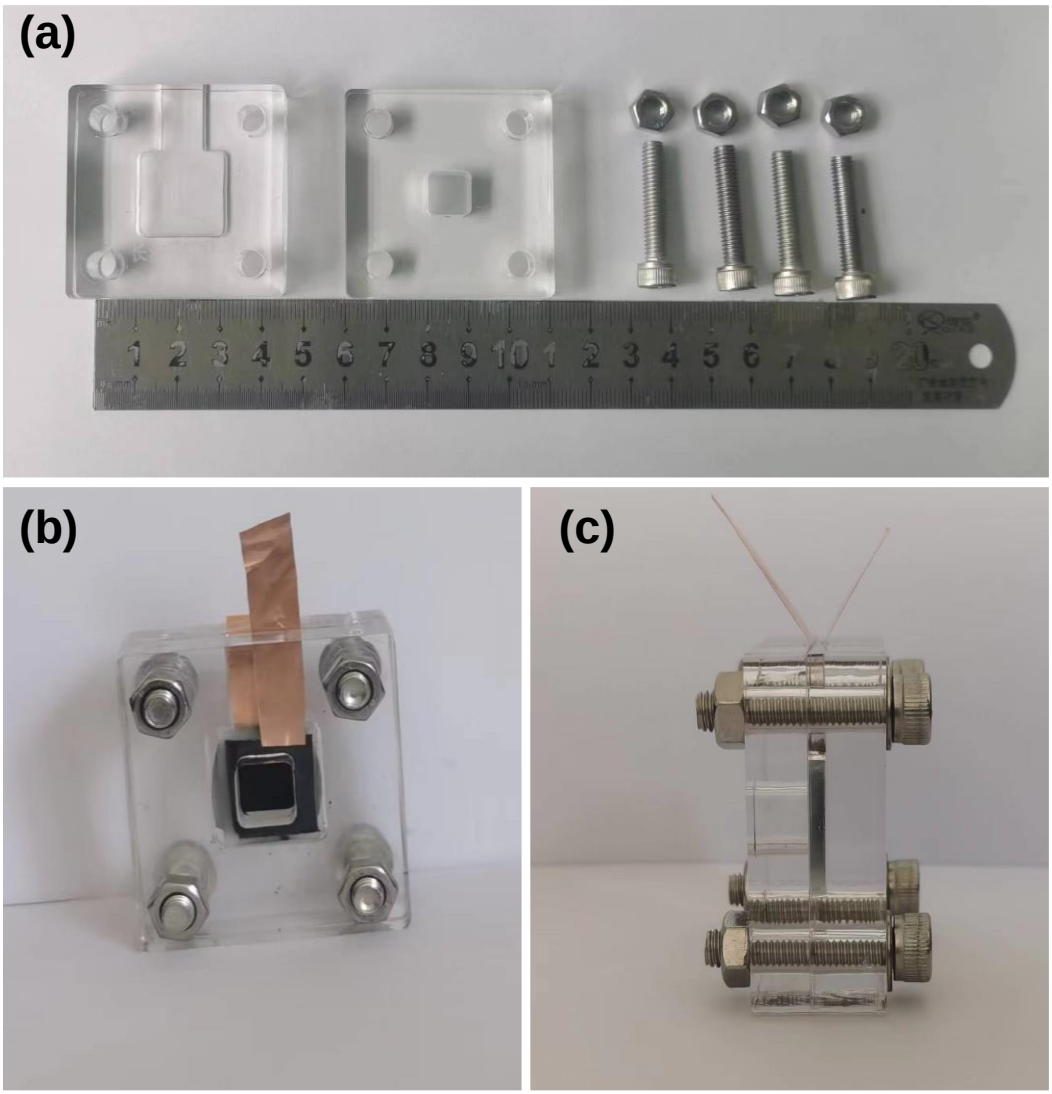

Fig. S18. (a) Optical photograph of plastic mold for assembling a FAZAB, and optical photographs of the PANa-PVP-$TiO_2(NH_2)$ GPE assembled quasi-solid-state FAZABs, taken from (b) Front and (c) Side.

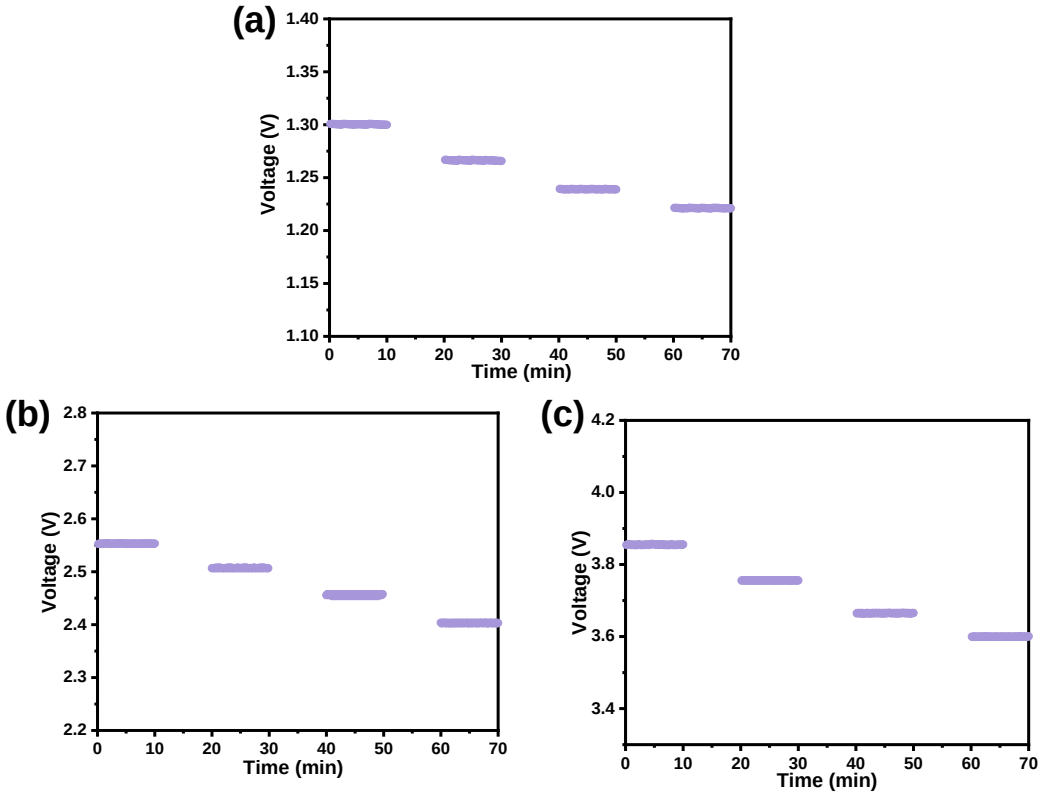

Fig. S19. Rate performances of the (a) One, (b) Two, and (c) Three series-connected batteries (The picture of one assembled PANa-PVP-$TiO_2(NH_2)$ GPE FAZAB is depicted in Fig.S15) at different current densities (2, 5, 10, and 15 mA cm^{-2}).

Table S1. Mechanical properties of PANa, PANa-PVP, PANa-$TiO_2(NH_2)$, and PANa-PVP-$TiO_2(NH_2)$ GPEs.

Samples	Elongation (%)	Tensile strength (KPa)
PANa	220	15.8
PANa-PVP	212	58
PANa-$TiO_2(NH_2)$	308	45
PANa-PVP-$TiO_2(NH_2)$	339	49

Table S2. Peak intensity ratio of ZnO/Zn on zinc plates according to XRD results.

Samples	Peak intensity of 34.5°(ZnO)	Peak intensity of 43.3°(Zn)	Peak intensity ratios of 34.5°/43.3°
Cycled Zn with PVA-KOH GPE	27705	34642	0.80
Cycled Zn with PANa GPE	14799	45640	0.32
Cycled Zn with PANa-PVP-$TiO_2(NH_2)$ GPE	1407	115550	0.012

Table S3. Performance of symmetric cell of PANa-PVP-TiO2(NH2) GPE compared with other GPEs.

Electrolyte	Current density (mA cm^{-2})	Time (h)	Ref.
PANa-PVP-$TiO_2(NH_2)$	1 mA cm^{-2}	348	This work
PANa-PVP-$TiO_2(NH_2)$	5 mA cm^{-2}	300	This work
PANa-PVP-$TiO_2(NH_2)$	10mA cm^{-2}	270	This work
PAM-SC	1 mA cm^{-2}	45	[5]
PAM-PEGMA-IL	0.1 mA cm^{-2}	250	[6]
GAE	0.2 mA cm^{-2}	1300	[7]

Table S4. Cyclic voltage gaps of FAZABs based on PVA, PANa and PANa-PVP-$TiO_2(NH_2)$ GPEs.

Hydrogel Electrolyte	Charging and discharging voltages	Initial voltage gap ΔV_1 (V)	Charging and discharging voltages	Terminal voltage gap ΔV_2 (V)	Difference of $\Delta V(\Delta V_2-\Delta V_1$, V)
PVA	1.87	0.64	2.0	1.07	0.43
	1.23		0.93		
PANa	1.97	0.9	2.03	1.06	0.16
	1.09		0.97		
PANa-PVP-$TiO_2(NH_2)$	1.91	0.66	1.93	0.7	0.04
	1.25		1.16		

Table S5. Power density and ionic conductivity of PANa-PVP-$TiO_2(NH_2)$ GPE compared with the existing GPEs.

Electrolyte	**Ionic conductivity (mS cm^{-1})**	**Power density (mW cm^{-2})**	**Ref.**
PANa-PVP-$TiO_2(NH_2)$	272	236	**This work**
Porous PVA	57.3	62.6	[8]
Nano-SF-PAA	186	104.2	[9]
PANaH	81.6	144.6	[10]
Fiber	240	68.7	[11]
PVA-PAA	123	74	[12]
PAMPS-PAAm	92	56.8	[13]
PAM−PAZn-Ss	249	60	[14]
PAMNa-CMCS	145.63	120.87	[15]
SLS@PVA-SSE	20.09	71	[16]
SSHPE	112.5	95.52	[17]

References

1) Huang N, Xie Y, Sebo B, Liu Y, Sun X, Peng T, Sun W, Bu C, Guo S, Zhao X, Morphology transformations in tetrabutyl titanate–acetic acid system and sub-micron/micron hierarchical TiO2 for dye-sensitized solar cells, Journal of Power Sources, 2013, 242:848-854.
2) Li J, Huang N, Lv M, Su N, Li C, Huang Y, Wang Y, Zheng Y, Liu W, Ma T, Ye L. OER highly active encapsulants to improve the electrochemical anticorrosion of Fe–N–C for ultralong-lifespan and high-rate rechargeable zinc–air batteries. Energy & Environmental Science:Catalysis, 2023, 1:987-997.
3) Song Z, Ding J, Liu B, Liu X, Han X, Deng Y, Hu W, Zhong C. A rechargeable Zn–air battery with high energy efficiency and long life enabled by a highly water-retentive gel electrolyte with reaction modifier, Advanced Materials. 2020, 32:1908127.
4) Liu X, Men C, Zhang X, Li Q. An extraordinary sulfonated-graphenal-polymer-based electrolyte separator for all-solid-state supercapacitors, Small, 2016, 12:4973-4979.
5) Jiao M, Dai L, Ren H.-R, Zhang M, Xiao X, Wang B, Yang J, Liu B, Zhou G, Cheng H.-M. A polarized gel electrolyte for wide-temperature flexible zinc-air batteries, Angewandte Chemie International Edition, 2023, 62:e202301114.
6) Li H, Xu F, Li Y, Sun J, Self-healing ionogel-enabled self-healing and wide-temperature flexible zinc-air batteries with ultra-long cycling lives, Advanced Science, 2024, 11:2402193.
7) Wu K, Cui J, Yi J, Liu X, Ning F, Liu Y, Zhang J, Biodegradable gel electrolyte suppressing water-induced issues for long-life zinc metal anodes, ACS Applied Materials & Interfaces, 2022, 14:34612-34619.
8) Fan X, Liu J, Song Z, Han X, Deng Y, Zhong C, Hu W. Porous nanocomposite gel polymer electrolyte with high ionic conductivity and superior electrolyte retention

capability for long-cycle-life flexible zinc–air batteries, Nano Energy, 2019, 56: 454-462.

9) Fan X, Wang H, Liu X, Liu J, Zhao N, Zhong C, Hu W, Lu J. Functionalized nanocomposite gel polymer electrolyte with strong alkaline-tolerance and high zinc anode stability for ultralong-life flexible zinc–air batteries. Advanced Materials, 2023, 35:2209290.
10) Pei Z, Huang Y, Tang Z, Ma L, Liu Z, Xue Q, Wang Z, Li H, Chen Y, Zhi C. Enabling highly efficient, flexible and rechargeable quasi-solid-state zn-air batteries via catalyst engineering and electrolyte functionalization. Energy Storage Materials, 2019, 20:234-242.
11) Zhang P, Wang K, Zuo Y, Wei M, Pei P, Liu J, Wang H, Chen Z, Shang N. A flexible zinc-air battery using fiber absorbed electrolyte, Journal of Power Sources, 2022, 531:231342.
12) Li W, Wang Y, Liu R, Chen W, Zhang H, Zhang Z. Gel polymer-based composite solid-state electrolyte for long-cycle-life rechargeable zinc–air batteries, ACS Sustainable Chemistry & Engineering, 2023, 11:3732-3739.
13) Jiang D, Wang H, Wu S, Sun X, Li J. Flexible zinc–air battery with high energy efficiency and freezing tolerance enabled by DMSO-based organon hydrogel Electrolyte, Small Methods, 2022, 6:2101043.
14) Zheng W, Zhao Y, Zhang H, Zhang L, Zhang Z. Extending the cycle lifetime of solid-state zinc-air batteries by arranging stable zinc species channels, ACS Applied Materials & Interfaces, 2024, 16:8885-8894.
15) Shang Z, Zhang H, Qu M, Wang R, Wan L, Lei D, Li Z. High adhesion hydrogel electrolytes enhanced by multifunctional group polymer enable high performance of flexible zinc-air batteries in wide temperature range, Chemical Engineering Journal, 2023, 468:143836.
16) Zhao P, Zhang L, Chen J, Qiu C, Wang B, Li J, Zhang K, Yang G. From wood to flexible Zn-air Battery: Fe3O4 nanoparticles synergistic single iron atoms on N-doped carbon nanosheets electrocatalyst and lignosulfonate-functionalized gel electrolyte, Chemical Engineering Journal, 2024, 484:149415.

17) Fan X, Zhang R, Sui S, Liu X, Liu J, Shi C, Zhao N, Zhong C, Hu W. Starch-based superabsorbent hydrogel with high electrolyte retention capability and synergistic interface engineering for long-lifespan flexible zinc−air batteries, Angewandte Chemie International Edition, 2023, 62:e202302640.